Particle Deformation and Concentration Polarization in Electroosmotic Transport of Hydrogels through Pores

Matthew Pevarnik,[†] Matthew Schiel,[†] Keiichi Yoshimatsu,[‡] Ivan V. Vlassiouk,[§] Jasmine S. Kwon,[‡] Kenneth J. Shea,[‡] and Zuzanna S. Siwy[†,*]

[†]Department of Physics and Astronomy, University of California, Irvine, California 92697, United States, [‡]Department of Chemistry, University of California, Irvine, California 92697, United States, and [§]Oak Ridge National Laboratory, Oak Ridge, Tennessee 37831, United States

ABSTRACT In this article, we report detection of deformable, hydrogel particles by the resistive-pulse technique using single pores in a polymer film. The hydrogels pass through the pores by electroosmosis and cause formation of a characteristic shape of resistive pulses indicating the particles underwent dehydration and deformation. These effects were explained *via* a non-homogeneous pressure distribution along the pore axis modeled by the coupled Poisson–Nernst–Planck and Navier–Stokes equations. The local pressure drops are induced by the electroosmotic fluid flow. Our experiments also revealed the importance of concentration polarization in the detection of hydrogels. Due to the negative charges as well as branched, low-density structure of the hydrogel particles, the concentration of ions in the particles is significantly higher than in the bulk. As a result, when an electric field is applied across the membrane, a depletion zone can be created in the vicinity of the particle observed as a transient drop of the current. Our experiments using pores with openings between 200 and 1600 nm indicated the concentration polarization dominated the hydrogels' detection of pores wider than 450 nm. The results are of importance for all studies that involve transport of molecules, particles, and cells through pores with charged walls. The developed inhomogeneous pressure distribution can potentially influence the shape of the transported species. The concentration polarization changes the interpretation of the resistive pulses; the observed current change does not necessarily reflect only the particle size but also the size of the depletion zone that is formed in the particle vicinity.

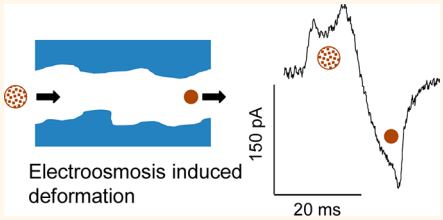

KEYWORDS: resistive-pulse technique · hydrogels · pore · deformation

Single-pore technology has been used to detect particles and detect their size. The approach works well for objects of very different sizes. Single nanopores with diameters less than 10 nm are used to detect single molecules such as DNA and proteins.[1−5] Pores with openings of several tens and several hundreds of nanometers were shown to detect viral capsids and particles.[6−12] Pores of micrometer size are routinely used in complete blood counts at hospitals. In all the above-mentioned cases, the species to be detected were in contact with one side of a single-pore membrane that separated two chambers of a conductivity cell filled with an electrolyte. Single molecules, particles, and cells were detected during their passage through the pore as a transient change in the recorded ion current called the resistive pulse.

Passing of particles through pores is also very important in the context of drug delivery, when considering particle clearance from the body. Hydrogels have become the center of interest since it was shown that by applying a pressure difference these deformable particles could pass through pores whose diameters were much smaller than the effective particle size.[13] If used as drug-delivery vehicles, these particles could therefore be cleared through the kidney system, which is known to contain nanopores with effective opening diameters of ~8 nm.[14] Clearing particles through the renal system is preferred since it prevents particle accumulation in the liver, which would otherwise lead to hepatoxicity.[14,15] Transport experiments of 116 nm diameter hydrogels were performed with polymer membranes containing multiple pores with an average opening of 10 nm.[13]

* Address correspondence to zsiwy@uci.edu.

Received for review February 15, 2013 and accepted March 29, 2013.

Published online April 01, 2013
10.1021/nn400774e

Detecting deformable particles with single pores could potentially provide more information than measurements with many-pore membranes. By studying resistive pulses one could learn about the dynamics of the particle deformation on a single-particle basis. Since multipore membranes contain pores with a finite distribution of the pore diameters, having one pore of known geometry allows one to understand the relation between the pore opening diameter and the pressure required for the particle deformation.[16−18] Studies with single man-made pores and hydrogels have been performed under an applied pressure difference using glass pipettes, with openings between 200 and 700 nm, and 570 nm diameter hydrogel particles.[16,17] Transport of single hydrogels led to the formation of a unique pattern of the resistive pulses consisting of a current increase followed by a current drop below the baseline value. Since the particles were largely filled with salt solution and additionally carried surface charges, their approach to the pore opening resulted in the increase of the measured transmembrane current. In order to squeeze through an opening that was smaller than the particle size, the particles had to deform and dehydrate, which was observed as a current decrease. The pulse shape was found to be dependent on the value of the applied pressure difference and the pore diameter. If the particles passed through sufficiently wide pipettes, the pulse consisted of only one positive peak, indicating that the presence of the particle in the pore lowered the system resistance.[16,17]

Nanopores in the kidneys are known to carry negative surface charges; thus it would also be of great interest to examine the effect of electrokinetic phenomena on the transport of deformable particles through pores.[19−21] In this article, we show that passage of hydrogel particles through pores with negative surface charges can indeed occur due to electroosmosis, without an additional pressure difference applied. Our measurements were performed with ∼300 nm diameter hydrogel particles and track-etched pores in polyethylene terephthalate (PET) with opening diameters between 200 and 1600 nm.[22,23] In all examined pores the recorded resistive pulses consisted of two distinct parts, one above and the other one below the baseline current, suggesting that the particles when in a pore underwent deformation/dehydration, and/or the ionic concentration in the particle and its proximity decreased below the bulk concentration. This is the first report showing particle dehydration in pores larger than the particle diameter, which is caused by the electric field instead of pressure. The results were explained by modeling ionic transport and electroosmosis-induced pressure profiles in charged pores using Poisson−Nernst−Planck and Navier−Stokes equations. Our results also point to the possibility of formation of a depletion zone in the vicinity of charged particles caused by concentration polarization, which dominates ionic transport through the pores.

The experiments were performed with polymer (PET) pores whose diameter is known to undulate along the pore axis.[24] Consequently, each pore produces a characteristic shape of resistive pulses that reflects local changes in the pore opening. The resistive-pulse shape allowed us therefore to elucidate at which location of the pore the dehydration and deformation of the particles occurred. Analysis of the data was facilitated by comparing the shape of resistive pulses corresponding to translocating hydrogels with the recordings performed in the presence of polystyrene particles, which behaved like hard spheres.

The results are of importance for all studies that involve transport of molecules, particles, and cells through pores with charged walls. This is because the experiments and modeling revealed the existence of a non-homogeneous pressure profile along the pore axis, which might affect the geometry of the detected species. In addition, when studying transport of highly charged molecules and particles, it is also important to consider the influence of concentration polarization on ionic transport.

RESULTS AND DISCUSSIONS

Figure 1 compares the passage of two types of particles, 220 nm diameter carboxyl-modified polystyrene beads and ∼300 nm diameter hydrogels, through a 12 μm long track-etched PET pore with an opening diameter of 540 nm. The size of all particles was measured using a Zetasizer Nano ZS (Malvern Instruments, Westborough, MA) as a function of ionic strength. The size of the polystyrene beads (220 nm) was found to be independent of the salt concentration. The diameter of the hydrogels was measured with 5% precision to be 320 nm, 300 nm, and 260 nm in 1 mM, 10 mM, and 0.1 M KCl, respectively. All KCl solutions were buffered to pH 10 with 10 mM Tris and contained 0.01% by volume Tween 80. At pH 10 the hydrogel particles are negatively charged and swollen due to the deprotonation of carboxyl groups in the hydrogel network.[25]

The polystyrene particles are a model system for hard spheres; thus, these particles do not deform in the pore. As expected, passage of the beads causes a transient decrease of the transmembrane ion current, called a resistive pulse, corresponding to a transient pore obstruction. The shape of the resistive pulses can also reflect the undulating pore diameter along the pore axis, as previously reported for PET pores.[24] The polystyrene particles therefore play a role of an internal probe of the pore topography. According to the shape of the resistive pulses, we predict that the pore shown in Figures 1 and 2 contains a larger cavity in the middle flanked by narrower regions of the pore. The presence of a brief current increase after each particle exits the

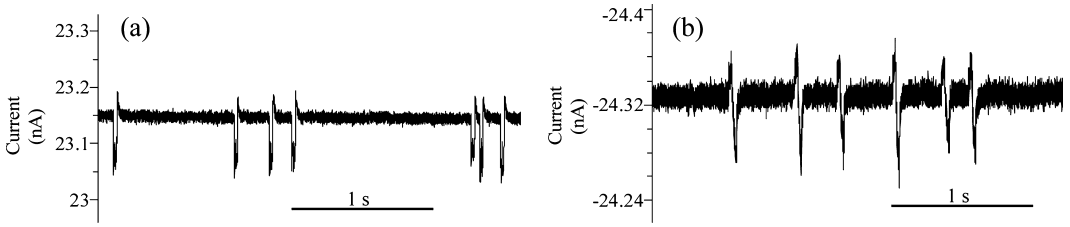

Figure 1. Ionic current *versus* time for a 540 nm diameter pore at (a) +1000 mV and (b) −1000 mV in 100 mM KCl, 10 mM Tris (pH 10), and 0.01% Tween 80: (a) 220 nm diameter hard spheres (polystyrene particles modified with carboxyl groups) translocate electrophoretically through the pore; (b) ~300 nm diameter hydrogels pass through the pore by electroosmosis.

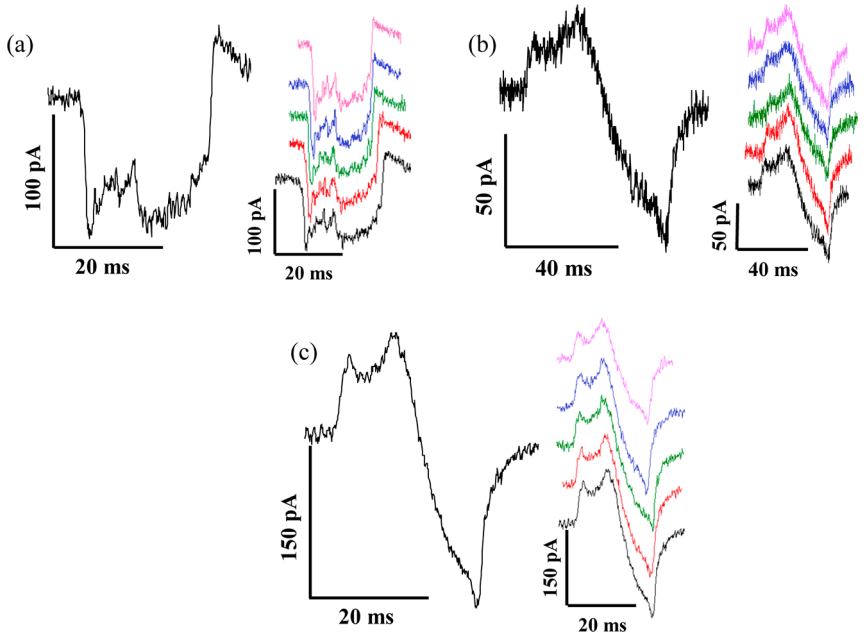

Figure 2. Magnified view of the ionic current pulses from Figure 1 for (a) the rigid spheres at +1000 mV, (b) the hydrogel particles at −1000 mV, and (c) the hydrogel particles at −2000 mV. A single event is shown on the left, while the right shows five events, vertically offset from each other to facilitate comparison.

pore could be explained by a rapid release of ions that accumulated near the pore mouth, as observed before in experiments of passing DNA molecules.[26,27] We assume ion current modulations within a resistive pulse are indeed indicative of the undulating pore diameter and not voltage-induced pore deformation. If the electrokinetic phenomena caused structural deformations, we would expect the resistive pulse to change its shape with the increase of the applied voltage and decrease of the bulk electrolyte concentration.[28] Such dependence was not observed in our system (Figures S1 and S2), which supports the hypothesis that current modulations within resistive pulses carry information about pore topography. Transport of polystyrene particles occurred by electrophoresis, where the negatively charged particles moved toward a positively biased electrode.

The hydrogel particles are characterized by a lower value of the zeta potential (-24 ± 8.0 mV) compared to the polystyrene beads (-47 ± 9.0 mV), and the hydrogels were able to pass through the same pore only by electroosmosis. The particles, although negatively charged, moved toward the negatively biased electrode. Due to the negative charges as well as the branched, low-density structure of the hydrogels, the number of cations that the particles introduced into the pore was in fact higher than the number of ions that were displaced. In other words, the hydrogel conductance in 100 mM KCl (and in 10 mM KCl; see below) is higher than the conductance of the bulk solution. As a result, the presence of the particles at the pore entrance and in the pore caused a decrease of resistance of the particle/pore system, leading to a higher value of the current compared to the baseline. The shape of the current pulses was similar to the one obtained with the polystyrene particles, except instead of a current decrease, a current increase was seen (Figure 2). The features of the resistive pulses with hydrogels were often better resolved at higher voltages compared to the experiments performed with hard spheres, because the current increase had a relatively small amplitude; thus higher voltages improved the signal-to-noise ratio.

In the course of the particle translocation however, typically at the end of the trajectory, the current

gradually decreased to a level below the background current. A similar shape of the current events, i.e., current increase followed by a decrease, was observed before in the experiments of pressure-driven passage of deformable microgels through glass pipettes.[16,17] The current decrease occurred only in previous experiments in which the pipet diameter was smaller than the particle size and was explained as a combination of particle deformation and dehydration. Observation of the current decrease with 300 nm particles passing through a 540 nm diameter pore was thus surprising for us.

In some cases, 2 out of 15, the current decrease occurred in the middle of the translocation process rather than at the end of the particle trajectory, as shown in Figure S3. The location of the particle could be determined since only part of the pore structure seen with polystyrene particles was observed in the pulses of the hydrogels.

In order to determine which processes were responsible for the current increase and decrease seen during hydrogel translocations, similar experiments to those shown in Figure 1 were performed with pores of different opening diameters between 200 and 1600 nm. The pore with an average diameter of 330 nm was the smallest structure through which the hydrogel passage was observed. In all experiments, hydrogel transport occurred only by electroosmosis; no electrophoretic translocations of hydrogels were recorded. The shape of the current changes was qualitatively the same for all pores (*i.e.*, a current increase followed by a decrease below the baseline value), independent of their diameter (Figure S4).

The resistive pulses were first analyzed by the amplitude of the current decrease, which is a measure of the particle size if we assume that the particle underwent a complete dehydration and deionization. Compression of the particles would decrease their volume and conductivity; thus the effective size would correspond to a sphere smaller than the original particle size. Figure 3 presents an average effective particle diameter as found from resistive pulses (the lowest recorded current) obtained with 300 nm hydrogels passing through pores with various opening diameters. The smaller effective diameter of the particle in pores with openings between 300 and 450 nm suggests that when translocating the hydrogels underwent both processes of deformation and dehydration.

The hydrogel dehydration and deformation was observed before only in pressure-driven experiments;[16,17] therefore we asked the question whether electroosmotic flow through our pores could potentially result in an inhomogeneous pressure distribution along the pore axis. The modeling was performed by numerically solving the coupled Poisson–Nernst–Planck (PNP) and Navier–Stokes (NS) equations (Comsol Multiphysics), as reported before.[29] Two types of structures were

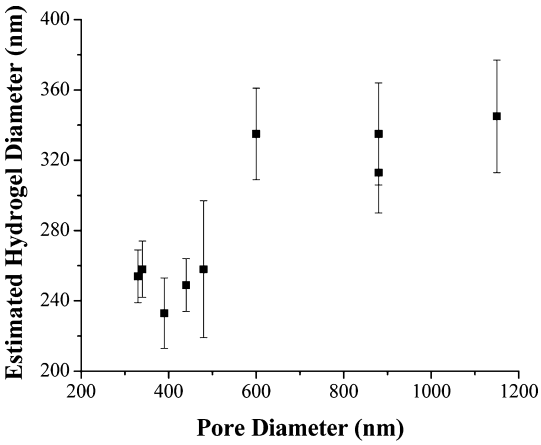

Figure 3. Size of the hydrogels as a function of the pore diameter. The hydrogel diameter was estimated from the depth of the resistive pulses in 10 mM KCl, pH 10, and 0.01% Tween 80 and calculated as described in ref 7. The hydrogel hydrodynamic diameter as measured by dynamic light scattering was 300 nm at 20 °C (10 mM KCl, pH 10).

considered: a smooth cylindrically shaped pore and a pore containing a wider cavity in the middle. The existence of such cavities was confirmed by preparing a metal replica of pores in PET.[24] The calculations required rather extensive computational power, because to ensure convergence of the solutions, the mesh size close to the charged walls had to be reduced to 0.1 nm. The maximum length of the modeled pores was therefore 1.5 μm (*versus* 12 μm length of the pores used in the experiments) to make solving PNP and NS equations in 3D possible. In order to understand dependence of the solution on the pore length, the modeling was performed for three different values of pore length between 600 nm and 1.5 μm.

The obtained pressure (with respect to atmospheric pressure) along the axis of two 1.5 μm long pores with different geometries is shown in Figure 4, where the direction of electroosmotic flow will be from +1 to 0 V, or from right to left. Due to undulating current amplitude within a resistive pulse (Figure 2), the structure shown in Figure 4b is a better representation of our experimental system. We interpret the results in the following way. The local negative pressure at the pore entrance can facilitate the particle translocation. Toward the pore exit, the local pressure is positive, which we think could play an important role in the particle deformation and dehydration. The absolute values of the pressure were substantially affected by the presence of the wider cavity, and the change in the pressure from negative to positive occurred over a smaller distance in the structure with varying pore diameter.

The developed pressure profile results from the electroosmotic fluid flow, which in turn depends on the electric field across the pore. It was important therefore to understand the dependence of the pressure distribution on the pore length. Figure 5a presents

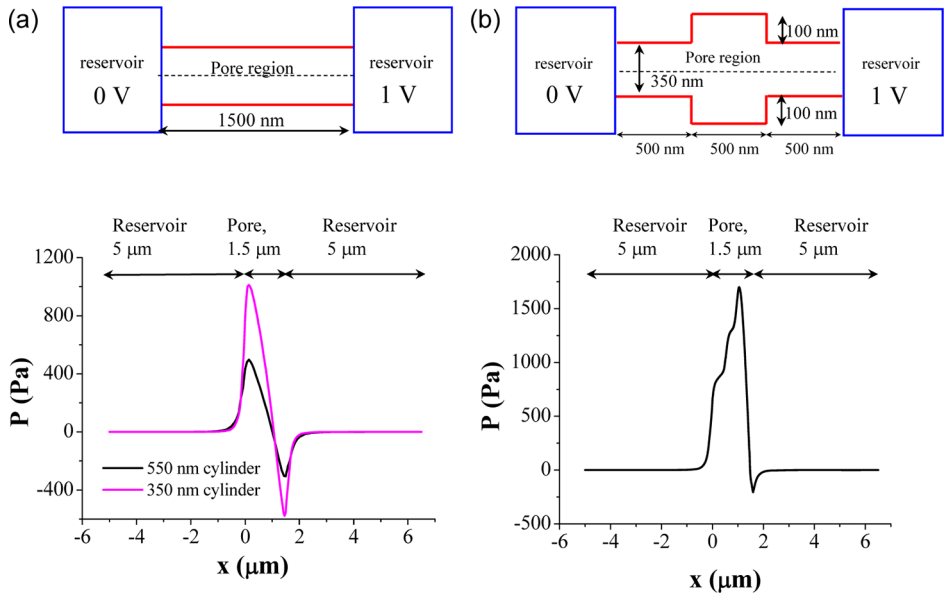

Figure 4. Modeling of pressure profile in 1.5 μm long pores that carry a surface charge of -0.25 e/nm^2. Results for (a) two cylindrically shaped pores with an opening diameter of 350 and 550 nm and (b) a pore with an undulating pore diameter between 350 and 550 nm are shown. Electroosmotic flow consisted of cations that moved from $+1$ to 0 V. The KCl bulk concentration was 10 mM. Pressure values with respect to the atmospheric pressure of 1 atm are shown.

numerical calculations of pressure along a pore axis for cylindrical pores with an opening diameter of 350 nm and lengths of 600 nm, 900 nm, and 1.5 μm. A voltage of 1 V was applied across all structures. The pressure profile was qualitatively the same for all pores; however the maximum value of positive pressure decreased with the increase of the pore length. The positive pressure in 12 μm long structures used in the experiments is therefore expected to be lower than the calculated values.

In contrast to the results for cylindrical pores, structures with an undulating pore diameter showed very little dependence of the maximum magnitude of the positive pressure on the pore length (Figure 5b). We think the pressure profile in this case is dominated by the boundary between the pore regions with two different opening diameters and to a lesser extent by the total pore length. It is possible therefore that even a 12 μm long pore has pressure values along the axis comparable to those found numerically for much shorter pores.

Two zones of negative and positive pressure, respectively, were predicted before to occur in a nanofluidic ionic transistor in which two regions of the channel walls with negative surface charges were separated by a neutral region or a positively charged region.[30] We hypothesize that our pores with an undulating pore diameter could be equivalent to such systems with inhomogeneous surface charges with lower effective surface charge density at the regions with wider openings.

According to the model predictions, the values of the developed electroosmotic pressure are a function of the pore diameter and diminish for wider pores (Figure 4a). As a result, no significant particle dehydration or deformation is expected to occur in pores with an opening diameter greater than 450 nm (see Figure 3). The shape of the resistive pulses caused by hydrogel particles was however independent of the pore diameter. Moreover, the magnitude of the current decrease in wider pores was equivalent to a particle larger than the studied 300 nm diameter hydrogels (Figure 3). On the basis of these observations we concluded that the current decrease in wider pores is caused by a different phenomenon than deformation or dehydration.

In order to explain the shape of resistive pulses in pores with large opening diameters, we calculated the concentration of ions in the hydrogel particles and compared the values to the bulk concentration (Table 1). The calculations were performed on the basis of the positive peak of the resistive pulses, which carry information on the number of additional ions that each particle brings to the pore, and the hydrogel size as found from the dynamic light scattering measurements. The hydrogel detection was carried out in 10 mM KCl and 0.1 M KCl. Nearly for all experiments, the ionic concentration in the particle was 10 times higher than in the bulk. The similarity of these values is likely due to osmotic pressure equilibrium, with the ratio between the particle and the bulk remaining similar regardless of the bulk ionic concentration.

The large difference in ionic concentrations in the particle and in the bulk as well as higher mobility of ions *versus* the particle's mobility set the stage for the concentration polarization.[31] Since the hydrogels are

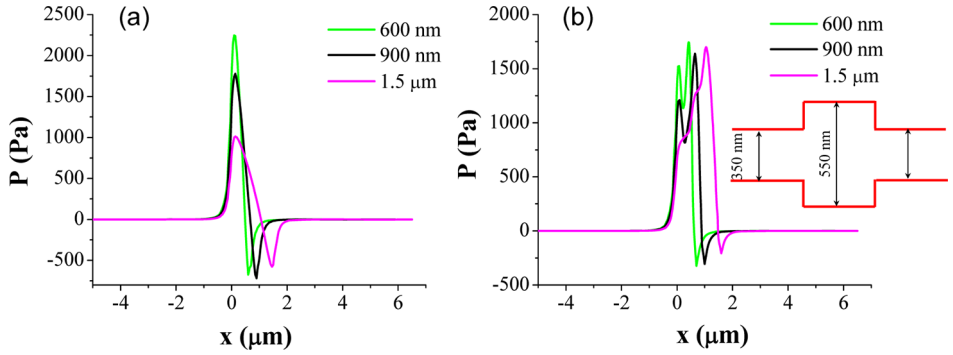

Figure 5. Modeling of pressure profile along the pore axis of a cylindrically shaped pore (a) and a pore with an undulating pore diameter, as shown in the inset (b). Both pores had a surface charge density of −0.25 e/nm^2, and the calculations were performed in 10 mM KCl of the background electrolyte. (a) Three cylindrically shaped pores with an opening diameter of 350 nm and lengths of 600 nm, 900 nm, and 1.5 μm were modeled. The reservoirs were 5 μm long, and the pore region started at the position 0 μm. Due to different lengths of the modeled pores, the right reservoir is positioned at different locations. (b) Three pores with undulating pore diameters were modeled. Two external zones with a 350 nm opening diameter and the middle zone with an opening of 550 nm were of equal length of 200, 300, and 500 nm in the 600 nm, 900 nm, and 1.5 μm long pores, respectively.

TABLE 1. Calculations of Ionic Molarity in Hydrogel Particles Based on Integrating Positive Peaks in Resistive Pulses Obtained in Pores of Different Diameters[a]

pore diameter, bulk concentration	molarity in the particle
330 nm, 0.01 M	0.11 ± 0.02 M
390 nm, 0.01 M	0.11 ± 0.03 M
440 nm, 0.01 M	0.06 ± 0.02 M
660 nm, 0.01 M	0.25 ± 0.06 M
500 nm, 0.1 M	1.03 ± 0.81 M
540 nm, 0.1 M	0.82 ± 0.24 M

[a] The hydrogel size as measured by the dynamic light scattering was used in the calculations.

moving in the same direction as potassium ions, there will be an ionic depletion at the back of the particle and ionic concentration enhancement in front of the translocating particle (Figure 6b). Concentration polarization was observed before in the vicinity of hydrogel plugs immobilized inside a microchannel.[32] In our case, the hydrogel is moving; thus we can conclude that the formation of the depletion zone is faster than the translocation velocity of the hydrogel.

Formation of the depletion zone would also explain why the current decrease occurred only toward the end of the particle passage through a pore. When the particle is close to the pore entrance, the influx of potassium ions to the particle is unhindered (Figure 6b). When the particle is moving along the pore axis and reaches the pore exit, the potassium ions have to be provided through the whole length of the pore, which plays a role of a resistive element. As a result, the concentration polarization becomes more pronounced once the particle reaches the opposite end of the pore.

The ion current decrease that we observe for pores with diameters larger than 450 nm is therefore a measure of the size of the depletion zone, which limits the ionic transport. We found the depletion zone diameter

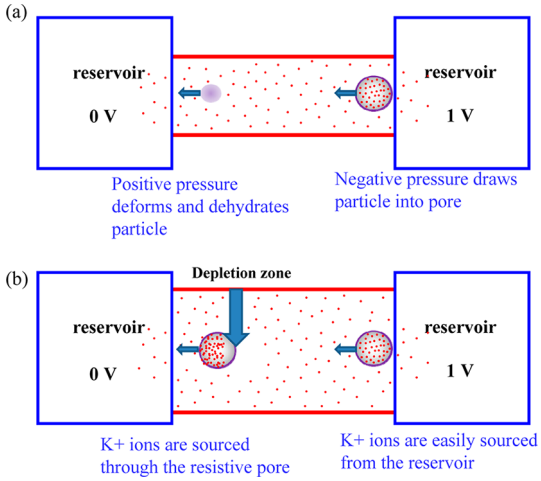

Figure 6. Scheme of electroosmotic passage of hydrogels through single pores. There are two different phenomena that lead to the decrease of ion current at the end of the particle translocation. (a) In pores with openings less than 450 nm, 300 nm hydrogel particles undergo deformation and dehydration; (b) in wider pores with openings greater than 450 nm, there is a depletion zone created in the vicinity of the particle.

(assuming it is spherical in shape) is independent of the pore size (Figure 3) and applied voltage in the studied range (up to 2 V; see Figure S5). It is also interesting that the depletion zone is larger than the translocating hydrogel particles. This observation is in agreement with earlier studies of concentration polarization showing the depletion zone can extend over large distances.[31] Our future experiments will be performed with hydrogels characterized by different surface charge densities, which are expected to influence the size of the depletion zone.

In order to provide additional evidence for the universal shape of resistive pulses obtained with hydrogels, we performed experiments with negatively charged pores in another polymer material, polycarbonate. The hydrogel particles passed through polycarbonate

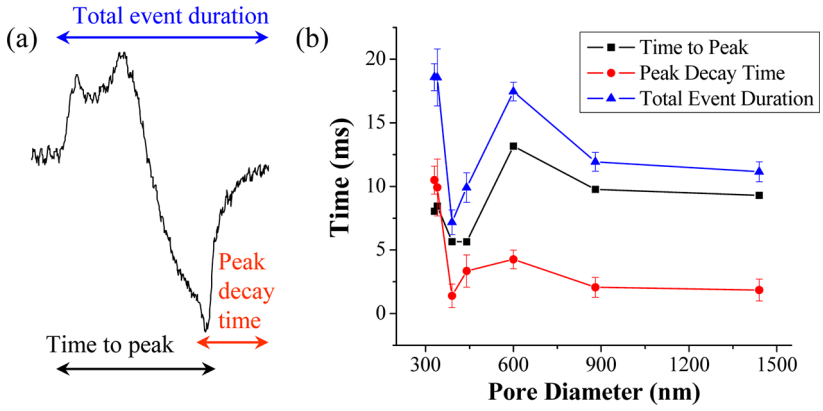

Figure 7. (a) Three times used to characterize duration of resistive pulses obtained with hydrogels translocating through pores of different diameters. The black symbols represent the time needed to reach the lowest value of the current, the red symbols indicate the time needed to reach the baseline current from the lowest value, and the blue symbols are the sum of the two. (b) Resistive pulse durations as shown in (a) for pores of different diameters recorded at −2 V. All experiments were performed in 10 mM KCl, pH 10, and 300 nm diameter hydrogels. Note that pulse durations of hydrogels are also a function of the bulk electrolyte concentration (Figure S2).

pores by electroosmosis as well, producing similarly shaped resistive pulses to those obtained with PET pores (Figure S6).

As the next step, we analyzed how the pore diameter influences the pulse duration, which is a measure of the particle velocity in the pore. In the case of hard spheres we and others observed an increase of the translocation time with a decrease of the pore diameter.[24,33] This is because particles experience an additional drag force stemming from the tight fit between the particle and the pore walls. The shape of the resistive pulses observed with hydrogels was more complex. To characterize their duration, three times were considered: (i) the time from the beginning of the pulse to the lowest current, (ii) the time from the lowest current value until it reaches the baseline current, and (iii) the total duration of the event, which is the sum of times (i) and (ii) (Figure 7a).

In general, the dependence of the translocation times of hydrogels on pore diameter does not follow a simple relationship. We believe this stems from the interplay between two phenomena, particle deformation and building up of a depletion zone, whose influence on the particle translocation is most probably dependent on the pore diameter. Our earlier analysis based on the magnitude of the current decrease (Figure 3, Figure 6) suggests that passage of hydrogels through narrow pores is dominated by the particle deformation; transport of the particles through wider pores leads to the formation of a depletion zone. The presented measurements however do not allow us to determine to what extent each of the two phenomena can affect hydrogel transport in a pore of a given diameter.

Our future experimental efforts will be focused on studying the passage of particles characterized by different levels of cross-linking, which is expected to lead to various mechanical properties of the particles, as well as particles with different numbers of ionizable groups. The additional measurements will allow us to understand which parts of the translocation process are mostly influenced by the particle deformation or by the depletion zone. Consequently, we will be able to map the influence of the two phenomena on the hydrogels' transport.

In spite of the complexity of Figure 7b, we would like to point to two important observations. Time (i), between the beginning of the pulse to the lowest value of the current, was found extremely reproducible: the black symbols in Figure 7b are averages of at least 500 pulses, and the error bars are smaller than the plot symbols. We do not yet have an explanation for this. Experiments with particles characterized by different levels of cross-linking will allow us to test whether time (i) can be correlated with mechanical properties of the particles.

Time (i) was also found to be longer for wider pores. This observation can be explained by taking into account the movement of both the particle and the depletion zone. The transported "object" is now larger than just the particle, and a higher drag force hinders its transport.

CONCLUSIONS

This article describes the electroosmotic transport of ~300 nm diameter hydrogel particles through single pores carrying negative surface charges. Passage of hydrogels caused formation of a characteristic shape of resistive pulses consisting of two parts, above and below the baseline current. The pulse shape was found to be independent of the pore diameter. The current increase in the beginning of the translocation process results from the higher conductance of the particles in comparison with the bulk solution so that the particles introduce additional ions to the pore. The current decrease at the end of the particle trajectory in the

pore indicates two different phenomena occurring in pores with different opening diameters. In structures with a diameter below 450 nm, the current decrease corresponds to dehydration and deformation of the particles. This conclusion was supported by numerical modeling, which revealed the existence of a nonhomogenous pressure profile along the pore axis resulting from electroosmotic fluid flow. This is the first report that shows hydrogel dehydration in pores that are larger than the particle size and induced by the electric field instead of a pressure difference. We hypothesize that in pores with an opening diameter of 450 nm and larger, the hydrogel transport is accompanied by the formation of a depletion zone in the vicinity of the particle. It is also very likely that the two phenomena, particle deformation/dehydration and building up of a depletion zone, affect the hydrogel transport in every pore to an extent that is dependent on the pore opening diameter.

The purpose of our report is also to point to the importance of the inhomogeneous pressure distribution created in charged pores for the detection of any nonrigid object, not only hydrogels but also biological cells. As we showed, resistive pulses can carry information on the particle deformation and/or formation of a depletion zone in the vicinity of the particle. In future resistive-pulse experiments, it will be therefore important to tune the pore diameter accordingly so that, for example, transported biological cells are not subjected to pressure inhomogeneities if the particular cell line is sensitive to local shear stresses. It will also be crucial to understand whether observed in a given system resistive pulses indeed reflect the particle size or rather the extent of the depletion zone adjacent to the translocating object.

Our future efforts will focus on resistive pulse experiments with hydrogels characterized by different levels of cross-linking. Our goal will be to develop a method to study mechanical properties of single particles based on their response to the pressure distribution along the pore axis and their ability to form depletion zones.

MATERIALS AND METHODS

Materials. All chemicals were obtained from commercial sources: potassium chloride (KCl), sodium hydroxide (NaOH), *N*-isopropylacrylamide (NIPAm), and ammonium persulfate (APS) were from Sigma-Aldrich, Inc. (St. Louis, MO); acrylic acid (AAc) and sodium dodecyl sulfate (SDS) were from Aldrich Chemical Co., Inc.; *N*,*N*′-methylenebisacrylamide (BIS) was from Fluka; *N*-*tert*-butylacrylamide (TBAm) was from Acros Organics (Geel, Belgium); NIPAm was recrystallized from hexane before use. Other chemicals were used as received. Water used in polymerization and characterization was distilled and then purified by using a Barnstead Nanopure Diamond system.

Track-Etched Pores. Single pores in 12 μm thick PET foils were used for the experiments presented here. Single pores prepared in 10 μm thick polycarbonate foils were used to collect data shown in Figure S6 in the Supporting Information. The pores were prepared by the track-etching technique consisting of irradiating the foils with single energetic heavy ions (*e.g.*, 11.4 MeV/u Au and U ions) at the UNILAC linear accelerator of the GSI Helmholtzzentrum für Schwerionenforschung, Darmstadt, Germany, and subsequent chemical etching.[22,23] PET foils were etched in 0.5 M NaOH, 70 °C, while polycarbonate was etched in 5 M NaOH, 50 °C. Under these etching conditions, the pores are characterized by an undulating pore diameter along the pore axis and are symmetric; that is, the pore opening diameter at both entrances is the same.[24] The mean pore diameter scales linearly with the etching time. The mean pore diameter can be estimated more precisely by measuring the pore conductance in a solution of known conductivity, based on the membrane thickness and the assumption of a cylindrical geometry. Walls of pores in PET and polycarbonate foils are known to carry negative surface charge due to the presence of carboxyl groups.[34]

Particles. The polystyrene particles used in these experiments were purchased from Bangs Laboratories, Fisher, IN, and all specifications quoted below were reported by the manufacturer. The carboxyl-functionalized (PS−COOH) particles used had nominal diameters of 120, 220, and 410 nm, with corresponding surface charge densities of −0.53, −1.10, and −3.66 e/nm^2. The zeta potential of the particles was measured in 10 M KCl, pH 10, 0.01% Tween 80 (Zetasizer Nano ZS, Malvern Instruments Ltd.).

The procedure reported by Debord and Lyon was adapted to synthesize hydrogel particles.[13,25] NIPAm (83 mol %), AAc (5 mol %), TBAm (10 mol %), BIS (2 mol %), and SDS (10 mg) were dissolved in water (50 mL), and the resulting solutions were filtered through a no. 2 Whatman filter paper. TBAm (10 mol %) was dissolved in ethanol (1 mL) before addition to the monomer solution. The total monomer concentration was 65 mM. Nitrogen gas was bubbled through the reaction mixtures for 30 min. Following the addition of APS aqueous solution (30 mg in 500 μL of water), the prepolymerization mixture was sealed under nitrogen gas. Polymerization was carried out by inserting the round bottle flask containing the prepolymerization mixture in an oil bath preset to 60 °C for 3 h. The polymerized solutions were purified by dialysis against an excess amount of pure water (changed twice a day) for 4 days.

Characterization of Hydrogel Particles. The yield and concentration of hydrogel particles were determined by gravimetric analysis of lyophilized hydrogel particles. The hydrodynamic diameter (D_H) of the hydrogel particles in buffer solutions was determined by a dynamic light scattering (DLS) instrument equipped with Zetasizer software ver. 6.12 (Zetasizer Nano ZS, Malvern Instruments Ltd.). The polystyrene latex beads were used as standard. All DLS data meet quality criteria set by Malvern. The intensity-weighted diameters of all three analyses were averaged and listed here. The zeta potential of the particles was measured in 10 mM KCl, pH 10, and 0.01% Tween 80.

For nuclear magnetic resonance (NMR) spectroscopy measurements (Figures S7, S8), 20 mg of lyophilized polymers was dissolved in 700 μL of CD_3OD and used. ^{1}H NMR and ^{13}C NMR were measured using a Bruker DRX500 spectrometer with a TCI (three channel inverse) cryoprobe. All measurements were run at 298 K, and the peak of residual CD_2HOD (δ 3.31 ppm for ^{1}H) and $^{13}CD_3OD$ (δ 49.15 ppm for ^{13}C) was used as a reference.

Ion Current Recordings and Analysis. Ion current signals were measured using an Axopatch 200B and a Digidata 1322A (Molecular Devices, Inc.). The ion current data were analyzed using Clampfit 9.0.

Modeling of Pressure Profiles. The numerical calculations of coupled Poisson−Nernst−Planck and Navier−Stokes equations were performed using the Comsol Multiphysics 4.3 package.[29] Modeled pores were connected with 5 μm long cylindrical reservoirs. A very fine triangular mesh of 0.1 nm was used close to the charged walls with a surface charge density

of -0.25 e/nm^2. In the remaining parts of the modeled structures, the mesh was reduced to the point where no change in the observed pressure profiles was observed upon further mesh decrease. The dielectric constant of the solution ($\varepsilon = 80$) and diffusion coefficients (2×10^{-9} m^2/s) were used for both potassium and chloride ions.

Conflict of Interest: The authors declare no competing financial interest.

Supporting Information Available: Examples of resistive pulses obtained with pores in polyethylene terephthalate and polycarbonate of different diameters together with NMR analysis of hydrogels are presented. This material is available free of charge *via* the Internet at http://pubs.acs.org.

Acknowledgment. Irradiation with swift heavy ions was performed at the GSI Helmholtzzentrum für Schwerionenforschung GmbH, Darmstadt, Germany. This research was supported by the National Science Foundation (CHE 0747237).

REFERENCES AND NOTES

1. Kasianowicz, J. J.; Brandin, E.; Branton, D.; Deamer, D. W. Characterization of Individual Polynucleotide Molecules Using a Membrane Channel. *Proc. Natl. Acad. Sci. U.S.A.* **1996**, *93*, 13770–13773.
2. Venkatesan, B. M.; Bashir, R. Nanopore Sensors for Nucleic Acid Analysis. *Nat. Nanotechnol.* **2011**, *6*, 616–624.
3. Cherf, G. M.; Lieberman, K. R.; Rashid, H.; Lam, C. E.; Karplus, K.; Akeson, M. Automated Forward and Reverse Ratcheting of DNA in a Nanopore at 5-Å Precision. *Nat. Biotechnol.* **2012**, *30*, 344–348.
4. Manrao, E. A.; Derrington, I. M.; Laszlo, A. H.; Langford, K. W.; Hopper, M. K.; Gillgren, N.; Pavlenok, M.; Niederweis, M.; Gundlach, J. H. Reading DNA at Single-Nucleotide Resolution with a Mutant MspA Nanopore and Phi29 DNA Polymerase. *Nat. Biotechnol.* **2012**, 349–354.
5. Movileanu, L. Squeezing a Single Polypeptide through a Nanopore. *Soft Matter* **2008**, *4*, 925–931.
6. Coulter, W. H. Means for Counting Particles Suspended in a Fluid. U.S. Pat. 2,656,508, 1953.
7. DeBlois, R. W.; Bean, C. P.; Wesley, R. K. A. Electrokinetic Measurements with Submicron Particles and Pores by the Resistive Pulse Technique. *J. Colloid Interface Sci.* **1977**, *61*, 323–335.
8. Berge, L. I.; Feder, J.; Jøssang, T. A Novel Method to Study Single-Particle Dynamics with Resistive Pulse Technique. *Rev. Sci. Instrum.* **1989**, *60*, 2756–2763.
9. DeBlois, R. W.; Bean, C. P. Counting and Sizing of Submicron Particles by the Resistive Pulse Technique. *Rev. Sci. Instrum.* **1970**, *41*, 909–916.
10. DeBlois, R. W.; Wesley, R. K. A. Sizes and Concentrations of Several Type C Oncornaviruses and Bacteriophage T2 by the Resistive-Pulse Technique. *J. Virol.* **1977**, *23*, 227–233.
11. Harms, Z. D.; Mogensen, K. B.; Nunes, P. S.; Zhou, K.; Hildenbrand, B. W.; Mitra, I.; Tan, Z.; Zlotnick, A.; Kutter, J. P.; Jacobson, S. C. Nanofluidic Devices with Two Pores in Series for Resistive-Pulse Sensing of Single Virus Capsids. *Anal. Chem.* **2011**, *83*, 9573–9578.
12. Zhou, K.; Li, L.; Tan, Z.; Zlotnick, A.; Jacobson, S. C. Characterization of Hepatitis B Virus Capsids by Resistive-Pulse Sensing. *J. Am. Chem. Soc.* **2011**, *133*, 1618–1621.
13. Hendrickson, G. R.; Lyon, L. A. Microgel Translocation through Pores under Confinement. *Angew. Chem., Int. Ed.* **2010**, *49*, 2193–2197.
14. Longmire, M.; Choyke, P. L.; Kobayashi, H. Clearance Properties of Nano-Sized Particles and Molecules as Imaging Agents: Considerations and Caveats. *Nanomedicine* **2008**, *3*, 703–717.
15. Choi, H. S.; Liu, W.; Misra, P.; Tanaka, E.; Zimmer, J. P.; Ipe, B. I.; Bawendi, M. G.; Frangioni, J. V. Renal Clearance of Quantum Dots. *Nat. Biotechnol.* **2007**, *25*, 1165–1170.
16. Holden, D. A.; Hendrickson, G. R.; Lan, W.-J.; Lyon, L. A.; White, S. H. Electrical Signature of the Deformation and Dehydration of Microgels during Translocation through Nanopores. *Soft Matter* **2011**, *7*, 8035–8040.
17. Holden, D. A.; Hendrickson, G.; Lyon, L. A.; White, H. S. Resistive Pulse Analysis of Microgel Deformation during Nanopore Translocation. *J. Phys. Chem. C* **2011**, *115*, 2999–3004.
18. Apel, P.; Korchev, Y. E.; Siwy, Z.; Spohr, R.; Yoshida, M. Diode-Like Single-Ion Track Membrane Prepared by Electro-Stopping. *Nucl. Instrum. Methods Phys. Res., Sect. B* **2001**, *184*, 337–346.
19. Deen, W. M.; Lazzara, M. J.; Myers, B. D. Structural Determinants of Glomerular Permeability. *Am. J. Physiol. Renal. Physiol.* **2001**, *281*, F579–F596.
20. Ohlson, M.; Sorensson, J.; Haraldsson, B. A Gel-Membrane Model of Glomerular Charge and Size Selectivity in Series. *Am. J. Physiol. Renal. Physiol.* **2001**, *280*, F396–F405.
21. Kobayashi, H.; Le, N.; Kim, I. S.; Kim, M. K.; Pie, J. E.; Drumm, D.; Paik, D. S.; Waldmann, T. A.; Paik, C. H.; Carrasquillo, J. A. The Pharmacokinetic Characteristics of Glycolated Humanized anti-Tac Fabs Are Determined by Their Isoelectric Points. *Cancer Res.* **1999**, *59*, 422–430.
22. Fleischer, R. L.; Price, P. B.; Walker, R. M. *Nuclear Tracks in Solids: Principles and Applications*; University of California Press: Berkeley, CA, 1975.
23. Spohr, R. Methods and Device to Generate a Predetermined Number of Ion Tracks. German Patent DE2951376 C2, Sept 15, 1983; U.S. Patent 4369370, 1983.
24. Pevarnik, M.; Healy, K.; Toimil-Molares, M. E.; Morrison, A.; Létant, S. E.; Siwy, Z. S. Polystyrene Particles Reveal Pore Substructure as They Translocate. *ACS Nano* **2012**, *6*, 7295–7302.
25. Debord, J. D.; Lyon, L. A. Synthesis and Characterization of pH-Responsive Copolymer Microgels with Tunable Volume Phase Transition Temperatures. *Langmuir* **2003**, *19*, 7662–7664.
26. Aksimentiev, A.; Heng, J. B.; Timp, G.; Schulten, K. Microscopic Kinetics of DNA Translocation through Synthetic Nanopores. *Biophys. J.* **2004**, *87*, 2086–2097.
27. Heng, J. B.; Ho, C.; Kim, T.; Timp, R.; Aksimentiev, A.; Grinkova, Y. V.; Sligar, S.; Schulten, K.; Timp, G. Sizing DNA Using a Nanometer-Diameter Pore. *Biophys. J.* **2004**, *87*, 2905–2911.
28. Ajdari, A. Electro-Osmosis in Inhomogeneosly Charged Surfaces. *Phys. Rev. Lett.* **1995**, *75*, 755–758.
29. Vlassiouk, I.; Smirnov, S.; Siwy, Z. S. Ion Selectivity of Single Nanochannels. *Nano Lett.* **2008**, *8*, 1978–1985.
30. Daiguji, H.; Oka, Y.; Shirono, K. Nanofluidic Diode and Bipolar Transistor. *Nano Lett.* **2005**, *5*, 2274–2280.
31. Zangle, T. A.; Mani, A.; Santiago, J. G. Theory and Experiments of Concentration Polarization and Ion Focusing at Microchannel and Nanochannel Interfaces. *Chem. Soc. Rev.* **2010**, *39*, 1014–1035.
32. Dhopeshwarkar, R.; Crooks, R. M.; Hlushkou, D.; Tallarek, U. Elektrokinetic Filtering with an Ion-Permselective Membrane. *Anal. Chem.* **2008**, *80*, 1039–1048.
33. Paine, P. L.; Scherr, P. Drag Coefficients for the Movement of Rigid Spheres through Liquid-Filled Cylindrical Pores. *Biophys. J.* **1975**, *15*, 1087–1091.
34. Ermakova, L. E.; Sidorova, M. P.; Bezrukova, M. E. Filtration and Electrokinetic Characteristics of Track Membranes. *Colloid J.* **1998**, *52*, 705–712.